(TE) was 4.2 ms, the flip angle was 20°, section thickness was 8 mm, and a 256 × 128 matrix was used. The acquisition time was 1.0 s, followed by an interval of 0.5 s. The 20 tumor contours extracted during 30 s were superimposed on sagittal and coronal MR images. The maximum value of tumor edge location was 3.9 cm in the CC direction, 2.3 cm in the AP direction, and 3.1 cm in the RL direction. The mean length of tumor displacement observed was 2.1 cm in the CC direction, 0.8 cm in the AP, and 0.9 cm in the RL direction. The locus of the center of the tumor contour in the sagittal cross-section was inclined at 23° to the craniocaudal axis of the body, and in the coronal cross-section, this locus was inclined at 18°.

Shimizu et al.[12] have reported that 4D treatment planning has the potential to determine the planning target volume of moving body tumors more precisely than does conventional CT planning. High-speed MRI was applied to the determination of the PTV of moving hepatobiliary tumors. Three moving tumors – two metastatic hepatic tumors and one bile duct tumor – were examined using high-speed MRI and reference fiducial markers before external radiotherapy. Patients were examined for 30 s under conditions of normal breathing during the examination. The coordinates of the center of the tumor contours were shown on sagittal and coronal images displayed on the monitor. The maximum length of movement was 10.6 ± 7.0 mm in the CC direction; 5.2 ± 1.8 mm in the RL direction; and 4.6 ± 1.6 mm in the ventrodorsal direction. When the PTV was determined using MRI in the exhalation phase, with a 10-mm safety margin, the clinical target volume (CTV) was not covered in 19% of all images in the three patients. With MRI in the inhalation phase with a 10-mm safety margin, CTV was not covered in 36% of all images.

Kitamura et al.[13] investigated the 3D intrafractional motion of liver tumors using the RTRT system. Tumor location, cirrhosis, and history of surgery on the liver all had an impact on the intrafractional tumor motion of the liver in the transaxial direction. The data of 20 patients with liver tumors were analyzed. Before treatment, a 2-mm gold marker was implanted near the tumor. Each of the following clinical factors was evaluated to determine its contribution to the amplitude of movement: tumor position, existence of cirrhosis, surgical history, tumor volume, and distance between the isocenter and the marker. The average amplitude of tumor motion in the 20 patients was 4 ± 4 mm (range, 1–12 mm) in the RL direction, 9 ± 5 mm (range, 2–19 mm) in the CC direction, and 5 ± 3 mm (range, 2–12 mm) in the AP direction. The tumor motion of the right lobe was significantly larger than that of the left lobe in the left-right and AP directions ($P = 0.01$). The tumor motion in the left-right and AP directions in the patients with liver cirrhosis was significantly larger than that in the patients without liver cirrhosis ($P < 0.004$). The tumor motion in the left-right and AP directions in the patients who had received a partial hepatectomy was significantly smaller than that in the patients who had no history of any operation on the liver ($P < 0.03$). Thus, three of the five clinical factors examined (i.e., tumor position in the liver, cirrhosis, and history of surgery on the liver) significantly affected the

tumor motion of the liver in the transaxial direction during stereotactic irradiation. Frequency analysis revealed that for 9 (45%) of the 20 tumors, the cardiac beat caused measurable motion. The 3D trajectory of the tumor showed hysteresis for 4 (20%) of the 20 tumors. The average treatment efficiency of RTRT was 40%.

Prostate motion

Shimizu et al.[14] have shown that the implantation of fiducial markers and the RTRT system can reduce uncertainty due to setup error and internal organ motion in the precise localization and verification of prostate and bladder cancers. The position of the patient can be corrected by adjusting the actual marker position to the planned marker position, which has been transferred from the 3D radiation treatment planning system and superimposed on the fluoroscopic image on the display unit of the RTRT system. Ten patients with prostate cancer and 5 patients with bladder cancer were examined for the treatment setup on 91 occasions. After manual setup using skin markers, the median absolute value of discrepancies between the actual position of the marker and the planned position of the marker for prostate cancer was 3.4 mm (range, 0.1–8.9 mm), 4.1 mm (range, 0.2–18.1 mm), and 2.3 mm (range, 0.0–10.6 mm) for the RL, AP, and CC directions, respectively. The 3D median distance between the actual and planned positions of the marker was 6.9 mm (range, 1.1–18.2 mm) for prostate cancer and 6.9 mm (range, 1.7–18.6 mm) for bladder cancer. After relocation using RTRT, the 3D distance between the actual and planned position of the marker was 0.9 ± 0.9 mm. Median 3D distances between actual positions for the marker after treatment delivery and planned positions during daily radiotherapy were 1.6 mm (range, 0.0–6.3 mm) and 2.0 mm (range, 0.5–8.0 mm) in patients with prostate cancer and bladder cancer, respectively.

Kitamura et al.[15] quantified 3D movement of the prostate gland with the patient in the supine and prone positions to analyze the movement frequency for each treatment position. In ten patients, the coordinates of the gold marker were recorded every 0.033 s for 2 min during RTRT with the patient in the supine treatment position. The patient was then moved to the prone position, and the marker was tracked for 2 min to acquire data regarding movement in this position. Measurements were taken five times for each patient (once a week); a total of 50 sets for the ten patients were analyzed. Discrete Fourier transform of the unfiltered data was performed for the frequency analysis of prostate movement. No apparent difference in movement was found among individuals. The amplitude of 3D movement was 0.1–2.7 mm in the supine and 0.4–24 mm in the prone position. The amplitude in the supine position was significantly smaller in all directions than that in the prone position ($P < 0.0001$). The amplitude in the CC and AP directions was larger than that in the RL direction in the prone position ($P < 0.0001$). No characteristic movement frequency was detected in the supine position. The respiratory fre-

quency was detected for all patients in the prone position regarding movement in the CC and AP directions. The results of the frequency analysis suggest that, in the prone position, prostate movement is affected by the respiratory cycle and is influenced by bowel movement. The results of this study have confirmed that, in the treatment of prostate cancer, internal organ motion is less frequent in the supine position than in the prone position. RTRT was suggested to be useful in reducing uncertainty due to the effects of the respiratory cycle, especially with patients in the prone position.

Early clinical results using the RTRT system and forward IMRT were reported by Kitamura et al.[16] Patients were classified into prognostic risk groups on the basis of the presence of pretreatment prostate-specific antigen, clinical stage, and histologic differentiation. Neoadjuvant hormonal therapy was administered to patients in the high-risk group for 6 months before radiation therapy commenced. The radiation dose was escalated in increments of 5 Gy from 65 Gy, using a daily dose of 2.5 Gy (65 Gy/2.5 Gy), following the dose-escalation rules. Acute and late gastrointestinal and genitourinary morbidities due to radiation therapy were scored according to the toxicity criteria of the Radiation Therapy Oncology Group (RTOG)/European Organization for Research and Treatment of Cancer. Eighteen patients were classified as being in the high-risk group. The total dose was escalated, with 65 Gy/2.5 Gy being administered to 12 patients and 70 Gy/2.5 Gy to 19 patients. The median follow-up period was 37 months (range, 30–43 months) for the 65-Gy arm, and 19 months (range, 10–27 months) for the 70-Gy arm. Patients in the 65-Gy/2.5-Gy arm experienced no acute toxicity and grade 1 late gastrointestinal toxicity (8.3%). Patients in the 70-Gy/2.5-Gy arm experienced grade 1 acute gastrointestinal toxicity (5.3%) and grade 1 and 2 acute genitourinary toxicities (15.8%). In this study period, no patients experienced dose-limiting toxicity (defined as a grade 3 or higher acute toxicity) or a grade 2 or higher late complication. One prostate-specific antigen relapse was observed in the 65-Gy arm and two prostate-specific antigen relapses were observed in the 70-Gy arm. Up to 70 Gy/2.5 Gy IMRT – equivalent to 80 Gy with a daily dose of 2.0 Gy – assuming an alpha/beta ratio of 1.5 – assisted by the RTRT system, was administered safely with a reasonable biochemical control rate.

Spinal schwannoma

The efficacy of the RTRT system, using three gold markers for estimating translational error, rotational setup error, and the dose to normal structures, was tested in five patients with spinal schwannoma, and a phantom.[17] Translational error was calculated by comparing the actual position of the marker closest to the tumor to its planned position, and the rotational setup error was calculated using the three markers around the target. Theoretically, the actual coordinates can be adjusted to the planning coordinates by sequential rotation of gamma° around the AP axis, beta° around the

CC axis, and alpha° around the RL axis, in this order. We measured the accuracy of the rotational calculation using a phantom. Five patients with spinal schwannoma located at a minimum of 1–5 mm from the spinal cord were treated with RTRT. Three markers were inserted percutaneously into the paravertebral deep muscle in three patients and surgically into two consecutive vertebral bones in the two other patients. In the phantom study, the mean discrepancy between the actual and calculated rotational error was –0.1 ± 0.5°. The random error of rotation was 5.9°, 4.6°, and 3.1° for alpha, beta, and gamma, respectively. The systematic error was 7.1°, 6.6°, and 3.0° for alpha, beta, and gamma, respectively. The mean rotational setup error (0.2 ± 2.2°, –1.3 ± 2.9°, and –1.3 ± 1.7° for alpha, beta, and gamma, respectively) in the two patients for whom surgical marker implantation was used was significantly smaller than that in the three patients for whom percutaneous insertion was used (6.0 ± 8.2°, 2.7 ± 5.9°, and –2.1 ± 4.6° for alpha, beta, and gamma). Random translational setup error was significantly reduced by the RTRT setup ($P < 0.0001$). Systematic setup error was significantly reduced by the RTRT setup only in those patients who received surgical implantation of the marker ($P < 0.0001$). The maximum dose to the spinal cord was estimated to be 40.6–50.3 Gy after consideration of the rotational setup error, vs a planned maximum dose of 22.4–51.6 Gy. Surgical implantation of the marker into the vertebral bone was shown to be sufficiently rigid for the calculation of the rotational setup error. Fractionated radiotherapy for spinal schwannoma using the RTRT system may well be an alternative or supplement to surgical treatment.

Gynecological malignancies

The feasibility and accuracy of high-dose 3D conformal boost (3DCB), using three internal fiducial markers and a two-orthogonal X-ray setup of the RTRT system in patients with gynecological malignancies, were investigated in ten patients by Yamamoto et al.[18] The SD of the distribution of systematic deviations (Σ) was reduced from 3.8, 4.6, and 4.9 mm for the three markers in the manual setup to 2.3, 2.3, and 2.7 mm in the setup using the internal markers. The average SD of the distribution of random deviations (sigma) was reduced from 3.7, 5.0, and 4.5 mm for the three markers in the manual setup to 3.3, 3.0, and 4.2 mm in the marker setup. The appropriate PTV margin was estimated to be 10.2, 12.8, and 12.9 mm for the three markers in the manual setup and 6.9, 6.7, and 8.3 mm in the gold marker setup, using the formula $2\Sigma + 0.7$ sigma. The setup of patients with three markers and a two-orthogonal X-ray is useful to reduce the PTV margin and to perform 3DCB.

Esophagus

Hashimoto et al.[19] evaluated the feasibility of real-time monitoring of a fiducial marker in/near the digestive tract

to analyze the motion of organs at risk to determine a reasonable internal margin. They developed two methods to insert a fiducial marker into/near the digestive tract adjacent to the target volume. One method involved an intraoperative insertion technique, and the other involved endoscopic insertion into the submucosal layer of the normal digestive tract. Fourteen markers (2 in the mediastinum and 12 in the abdomen) were implanted intraoperatively in 14 patients with no apparent migration. Seventeen of 20 markers (13/14 in the esophagus, 1/2 in the stomach, and 3/4 in the duodenum) were implanted in 18 patients, using endoscopy, without dropping. No symptomatic adverse effects related to insertion were observed. The mean/SD values for the range of motion of the esophagus were 3.5/1.8, 8.3/3.8, and 4.0/2.6 mm for the RL, CC, and AP directions, respectively, in patients with intrafractional tumor motion less than 1.0 cm. They concluded that both the intraoperative and the endoscopic insertions of a fiducial marker into/near the digestive tract for the monitoring of organs at risk were feasible, and the margin for internal motion could be individualized using the RTRT system.

Head and neck

To reduce setup error and intrafractional movement in head-and-neck treatment, gold markers implanted in a mouthpiece were used in RTRT by Oita et al.[20] Three 2-mm gold markers were implanted into a mouthpiece that had been custom made for each patient before the treatment planning process. Setup errors in the conventional immobilization system using the shell (manual setup) and the RTRT system (RTRT setup) were compared. Eight patients with pharyngeal tumors were enrolled. The systematic setup errors were 1.8, 1.6, and 1.1 mm in the manual setup and 0.2, 0.3, and 0.3 mm in the RTRT setup in the RL, CC, and AP directions, respectively. Statistically significant differences were observed with respect to the variances in setup error ($P < 0.001$). The systematic and random intrafractional errors were maintained within the ranges of 0.2–0.6 mm and 1.0–2.0 mm, respectively. The rotational systematic and random intrafractional errors were estimated to be 2.2–3.2° and 1.5–1.6°, respectively. Oita et al.[20] concluded that the setup error and planning target volume margin could be significantly reduced using an RTRT system with a mouthpiece and three gold markers.

Pancreas

Ahn et al.[21] have reported the usage of RTRT for unresectable pancreatic cancer. Three patients were treated with intraoperative electron-beam radiation therapy, at the time of open biopsy, and postoperative external-beam radiation therapy, using an RTRT system with a 2.0-mm diameter gold ball implanted into the pancreas. The total BED alpha/beta = 10 was intended to be equivalent to that of delivering 60 Gy by 2.0 Gy/fraction, while the actual dose schedules were individualized. During the RTRT course, the average movements of markers in the RL, CC, and AP directions were 3.0 mm (range, 1.7–5.2 mm), 5.2 mm (range, 3.5–6.8 mm), and 3.5 mm (range, 2.7–5.1 mm), respectively. During and after the course of postoperative radiation therapy, no acute side effects of RTOG grade II or higher were detected. The objective tumor responses, as evaluated by CT scans 3 months after the treatment, were two partial responses, and no response in one patient. Using the RTRT technique, the margin of treatment planning and the possible errors in target localization were reduced, and the 3D movement of the internal marker implanted in the pancreas was able to be analyzed.

Fiducial markers

The registration accuracy and possible migration of internal fiducial gold markers implanted into liver and prostate were investigated by Kitamura et al.[22] Internal fiducial gold markers were implanted in 14 patients with prostate cancer and 4 patients with liver tumors. Computed tomography (CT) was carried out as part of the treatment planning in these 18 patients. A total of 72 follow-up CT scans were taken. Kitamura et al.[22] calculated the relative relationship between the coordinates of the center of the mass (CM) of the organs and those of the marker. A discrepancy in the CM coordinates during a follow-up CT compared to those recorded during the planning CT was used to study possible marker migration. The SD of interobserver variations in the CM coordinates was within 2.0 mm and within 0.4 mm for the organ and the marker, respectively, in seven observers. Assuming that organs do not shrink, grow, or rotate, the maximum SD of migration error in each direction was estimated to be less than 2.5 mm for the liver and less than 2.0 mm for the prostate. Most of the marker movement could be attributed to measurement uncertainty, which also influences registration in actual treatment planning. Thus, these authors concluded that even with a gold marker and the RTRT system, a reasonable amount of PTV margin should be used to take into account registration uncertainty.

Equipment and techniques for the insertion of 2.0-mm-diameter gold markers into or near a tumor were improved to take into account rotational error and migration of the markers.[23] Three markers were used to adjust the CM of the target volume to the planned position in spinal/paraspinal lesions and prostate tumors (three-marker method). The feasibility of the marker insertion and the stability of the marker positions were tested using stopping rules in the clinical protocol (i.e., the procedure was abandoned if two of three or three of six patients experienced marker dropping or migration). After evaluation of the feasibility, the stability of the marker positions was monitored in those patients who entered the dose-escalation study. Each of

the following was shown to be feasible: bronchoscopic insertion for the peripheral lung; image-guided transcutaneous insertion for the liver; cystoscopic and image-guided percutaneous insertion for the prostate; and surgical implantation for spinal/paraspinal lesions. Transcutaneous insertion of markers for spinal/paraspinal lesions and bronchoscopic insertion for central lung lesions were abandoned. Overall, marker implantation was successful and was used for real-time tumor tracking in RT in 90 (90%) of 100 lesions. No serious complications related to the marker insertion were noted for any of the 100 lesions. Using three markers surgically implanted into the vertebral bone, the mean ± SD in distance among the three markers was within 0.2 ± 0.6 mm (range, −1.4 to 0.8 mm) throughout the treatment period of 30 days. The distance between the three markers gradually decreased during RT in five of six prostate cancers, consistent with a mean rate of volume regression of 9.3% (range, 0.015%–13%) in 10 days. The three-marker method has been shown to be a useful technique for precise setup for spinal/paraspinal lesions and prostate tumors.

The fixation rate of markers using the bronchial insertion technique, the reliability of the setup using markers around the target volume, dislocation of the markers after RTRT, and the long-term toxicity of marker insertion were investigated recently.[24] Between July 2000 and April 2004, 154 gold markers were inserted into 57 patients with peripheral lung cancer. The distances between the implanted markers in 198 measurements in 71 set-ups in 11 patients were measured using two sets of orthogonal diagnostic X-ray images of the RTRT system. The distance between the markers and the chest wall was also measured in a transaxial CT image on 186 occasions in 48 patients during treatment planning and during follow-up. The median treatment time was 6 days (range, 4–14 days). In 115 (75%) of the 154 inserted markers, the gold marker was detected throughout the treatment period. Of 122 markers detected at CT planning, 115 (94%) were detected until the end of treatment. The variation in the distances between the implanted markers was within ±2 mm in 95% and within ±1 mm in 80% during treatment. The variation in the distances between the implanted markers was more than 2 mm in at least one direction in 9% of the setups for which reexamination with a CT scan was indicated. The fixation rate in the left upper lobe was lower than that in the other lobes. A statistically significant relationship was found between a shorter distance between the markers and the chest wall and the fixation rate, suggesting that the markers in the smaller bronchial lumens fixed better than those in the larger lumens. A learning curve among the endoscopists was suggested in regard to the fixation rate. The distance between the markers and the chest wall changed significantly within a median of 44 days (range, 16–181 days) after treatment. The fixation of markers into the bronchial tree was useful for setup for peripheral lung cancer and had an accuracy of ±2 mm during the 1- to 2-week treatment period. The relationship between the markers and tumor can change significantly after 2 weeks, suggesting that adaptive 4DRT is required.

3D Conformal setup, 4D setup, and external surrogate

Shirato et al.[25] have made a system correcting for the rotational error of the target without having to reposition the patient, using three fiducial markers and two orthogonal fluoroscopic images. They called this system "three-dimensional conformal setup" (3D-CSU) and have reported its usefulness. The rotation angles (alpha, beta, gamma) of the coordinates of the actual CTV relative to the planned CTV are calculated around the RL (x), CC (y), and AP (z) axes of the planned CTV. The angles of the gantry head, collimator, and linear accelerator treatment couch are adjusted according to the rotation of the actual coordinates of the tumor in relation to the planned coordinates. The center of gravity of the phantom was corrected within 0.9 ± 0.3 mm (mean ± SD), 0.4 ± 0.2 mm, and 0.6 ± 0.2 mm for the rotation of the phantom from 0–30° around the RL, CC, and AP axes, respectively, every 5°. Dose distribution was shown to be consistent with the planned dose distribution every 10° of the rotation from 0° to 30°. The mean rotational error after 3D-CSU was −0.4 ± 0.4° (mean ± SD), −0.2 ± 0.4°, and 0.0 ± 0.5° around the RL, CC, and AP axes, respectively, for rotation from 0° to 90°. Phantom studies showed that 3D-CSU was useful for performing rotational correction of the target volume without correcting the position of the patient on the treatment couch. Shirato et al.[25] concluded that 3D-CSU would be clinically useful for paraspinal tumors and prostate cancers in regions not subject to large internal organ motion.

In 2005, Shirato et al.[26] developed a 4D setup system using a new RTRT system to reduce the uncertainty of registration for lung tumors. During treatment planning and daily setup in the treatment room, the trajectory of the internal fiducial marker was recorded for 1 to 2 min at the rate of 30 times per s. To maximize gating efficiency, the patient's position on the treatment couch was adjusted using the 4D setup system with fine online remote control of the treatment couch. The trajectory of the marker detected in the 4D setup system was well visualized and was used for daily setup (Fig. 3). Various degrees of interfractional and intrafractional changes in the absolute amplitude and speed of the internal marker were detected. Readjustments were necessary during each treatment session, prompted by baseline shifting of the tumor position. The 4D setup system was shown to be useful for reducing the uncertainty of tumor motion and for increasing the efficiency of gated irradiation. Considering the interfractional and intrafractional changes in speed and amplitude detected in this study, Shirato et al.[26] concluded that intercepting radiotherapy using the RTRT system was a safe and cost-effective method for 4DRT.

To mitigate motion-induced irradiation of normal lung tissue, clinics have employed external markers to gate the treatment beam. This technique assumes that the correlation between the external surface and the internal tumor position remains constant interfractionally and intrafractionally. Berbeco et al.[27] assessed the validity of this assumption of correlation for external surface-based gated

Fig. 3. Trajectory of a marker near a lung tumor in a patient with lung cancer before and after four-dimensional setup. Each spot corresponds to the position of the marker as detected by the real-time tumor-tracking radiotherapy system. In this case, Point P and the gating window (box) were set at the isocenter with 2 mm isotropical "permitted dislocation" from Point P. The actual position of the marker at the end of expiration, Point A, in the trajectory of the marker is adjusted to Point P by moving the treatment couch. The x, y and z are consistent with the right-left, craniocaudal, and anteroposterior directions, respectively

(a) Before 4D setup

(b) After 4D setup
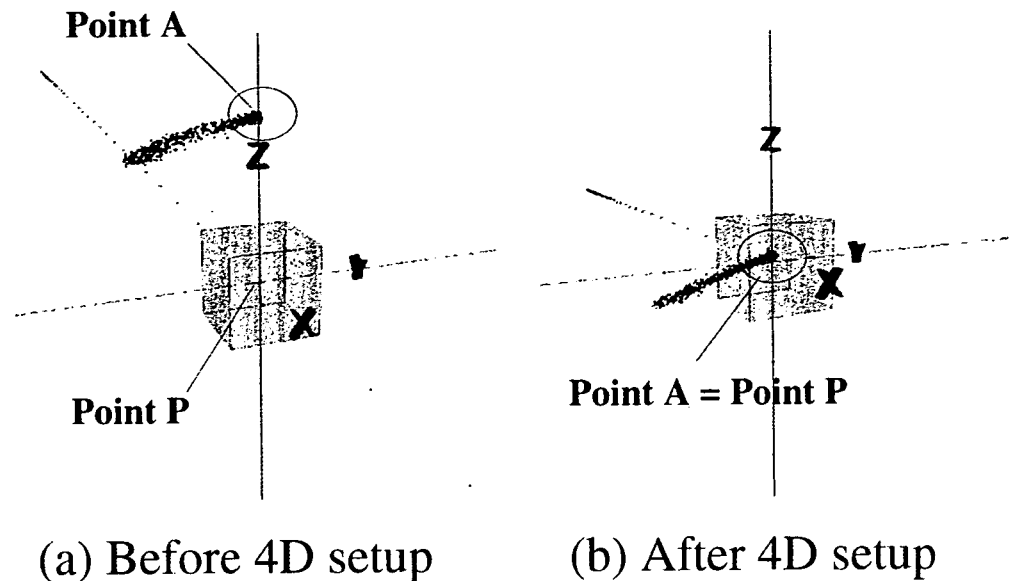
radiotherapy, by measuring the residual tumor motion within a gating window. Eight patients with lung tumors with implanted fiducial markers were studied at the NTT Hospital in Sapporo, Japan. Synchronized internal marker positions and external abdominal surface positions were measured during the entire course of treatment. Both amplitude- and phase-based gating methods were investigated. For each method, three gating windows were investigated, each giving a 40%, 30%, and 20% duty cycle, respectively. The residual motion of the internal marker within these six gating windows was calculated. The beam-to-beam variation and day-to-day variation in the residual motion were calculated for both gating modalities. Berbeco et al.[27] found that the residual motion (95th percentile) was between 0.7 and 5.8 mm, 0.8 and 6.0 mm, and 0.9 and 6.2 mm for the 20%, 30%, and 40% duty cycle windows, respectively. Five of the eight patients showed less residual motion with amplitude-based gating than with phase-based gating. Large fluctuations (>300%) were seen in the residual motion between some beams. Overall, the mean beam-to-beam variation from the previous treatment beam was 37% for amplitude-based gating and 42% for phase-based gating. The day-to-day variation from the previous day was 29% for amplitude-based gating and 34% for phase-based gating. Although gating reduced the total tumor motion, the residual motion behaved unpredictably. Residual motion during treatment could exceed that which might have been considered in the treatment plan. Treatment margins that take motion into account should be individualized, and daily imaging should be performed to ensure that the residual motion does not exceed the planned motion on a given day.

Concluding remarks

The benefit of the RTRT system in reducing the uncertainty in regard to setup and organ motion has been shown in the actual treatment of patients. Reports of the benefits of the RTRT system in improving the clinical outcome of RT have begun to be published recently, 5–7 years after the start of clinical trials. Several studies have shown that a predictive model of respiration may be useful to reduce the requirement for fluoroscopic monitoring during irradiation.[28] However, any risk of missing the CTV from the PTV must be avoided. We need to be careful about the residual error due to organ motion, which often cannot be predicted in IGRT.[29] Image is better than imagination, but an image is always different from the real.

References

1. Aoyama H, Shirato H, Tago M, et al. (2006) Stereotactic radiosurgery plus whole-brain radiation therapy vs stereotactic radiosurgery alone for treatment of brain metastases: a randomized controlled trial. JAMA 295:2483–2491

2. Uematsu M, Shioda A, Tahara K, et al. (1998) Focal, high dose, and fractionated modified stereotactic radiation therapy for lung carcinoma patients: a preliminary experience. Cancer 82:1062–1070

3. Jiang SB (2006) Technical aspects of image-guided respiration-gated radiation therapy. Med Dosim 31:141–151

4. Shirato H, Shimizu S, Shimizu T, et al. (1999) Real-time tumor-tracking radiotherapy. Lancet 353:1331–1332

5. Shimizu S, Shirato H, Kagei K, et al. (2000) Impact of respiratory movement on the computed tomographic images of small lung tumors in three-dimensional (3D) radiotherapy. Int J Radiat Oncol Biol Phys 46:1127–1133

6. Shirato H, Shimizu S, Kitamura K, et al. (2000) Four-dimensional treatment planning and fluoroscopic real-time tumor tracking radiotherapy for moving tumor. Int J Radiat Oncol Biol Phys 48:435–442

7. Shirato H, Shimizu S, Kunieda T, et al. (2000) Physical aspects of a real-time tumor-tracking system for gated radiotherapy. Int J Radiat Oncol Biol Phys 48:1187–1195

8. Shimizu S, Shirato H, Ogura S, et al. (2001) Detection of lung tumor movement in real-time tumor-tracking radiotherapy. Int J Radiat Oncol Biol Phys 51:304–310

9. Seppenwoolde Y, Shirato H, Kitamura Y, et al. (2002) Precise and real-time measurement of 3D tumor motion in lung due to breathing and heartbeat, measured during radiotherapy. Int J Radiat Oncol Biol Phys 53:822–834

16

10. Harada T. Shirato H. Obura S, et al. (2002) Real-time tumor-tracking radiation therapy for lung carcinoma by the aid of insertion of a gold marker using bronchofiberscopy. Cancer 95:1720–1727

11. Shimizu S. Shirato H, Xo B, et al. (1999) Three-dimensional movement of a liver tumor detected by high-speed magnetic resonance imaging. Radiother Oncol 50:367–370

12. Shimizu S. Shirato H. Aoyama H, et al. (2000) High-speed magnetic resonance imaging for four-dimensional treatment planning of conformal radiotherapy of moving body tumors. Int J Radiat Oncol Biol Phys 48:471–474

13. Kitamura K. Shirato H, Seppenwoolde Y, et al. (2003) Tumor location, cirrhosis, and surgical history contribute to tumor movement in the liver, as measured during stereotactic irradiation using a real-time tumor-tracking radiotherapy system. Int J Radiat Oncol Biol Phys 56:221–228

14. Shimizu S. Shirato H, Kitamura K, et al. (2000) Use of an implanted marker and real-time tracking of the marker for the positioning of prostate and bladder cancers. Int J Radiat Oncol Biol Phys 48:1591–1597

15. Kitamura Y, Shirato H, Seppenwoolde Y, et al. (2002) Three-dimensional intrafractional movement of prostate measured during real-time tumor-tracking radiotherapy in supine and prone treatment positions. Int J Radiat Oncol Biol Phys 53:1117–1123

16. Kitamura K. Shirato H, Shinohara N, et al. (2003) Reduction in acute morbidity using hypofractionated intensity-modulated radiation therapy assisted with a fluoroscopic real-time tumor-tracking system for prostate cancer: preliminary results of a phase I/II study. Cancer J 9:268–276

17. Onimaru R, Shirato H, Aoyama H, et al. (2002) Calculation of rotational setup error using the real-time tracking radiation therapy (RTRT) system and its application to the treatment of spinal schwannoma. Int J Radiat Oncol Biol Phys 54:939–947

18. Yamamoto R, Yonesaka a, Nishioka S, et al. (2004) High dose three-dimensional conformal boost (3DCB) using an orthogonal diagnostic X-ray set-up for patients with gynecological malignancy: a new application of real-time tumor-tracking system. Radiother Oncol 73:219–222

19. Hashimoto K, Shirato H, Katoh M, et al. (2005) Real-time monitoring of a digestive tract marker to reduce adverse effects of moving organs at risk (OAR) in radiotherapy for thoracic and abdominal tumors. Int J Radiat Oncol Biol Phys 61:1559–1564

20. Oita S, Ohmori K, Obinata K et al. (2006) Uncertainty in treatment of head-and-neck tumors by use of intraoral mouthpiece and embedded fiducials. Int J Radiat Oncol Biol Phys 64:1581–1588

21. Ahn YC. Shimizu S, Shirato H, et al. (2004) Application of real-time tumor-tracking and gated radiotherapy system for unresectable pancreatic cancer. Yonsei Med J 45:584–590

22. Kitamura K, Shirato H, Shimizu S, et al. (2002) Registration accuracy and possible migration of internal fiducial gold marker implanted in prostate and liver treated with real-time tumor-tracking radiation therapy (RTRT). Radiother Oncol 62:275–281

23. Shirato H, Harada T, Harabayashi T, et al. (2003) Feasibility of insertion/implantation of 2.0-mm-diameter gold internal fiducial markers for precise setup and real-time tumor tracking in radiotherapy. Int J Radiat Oncol Biol Phys 56:240–247

24. Imura M, Yamazaki K, Shirato H, et al. (2005) Insertion and fixation of fiducial markers for setup and tracking of lung tumors in radiotherapy. Int J Radiat Oncol Biol Phys 63:1442–1447

25. Shirato H, Oita M, Fujita K, et al. (2004) Three-dimensional conformal setup (3D-CSU) of patients using the coordinate system provided by three internal fiducial markers and two orthogonal diagnostic X-ray systems in the treatment room. Int J Radiat Oncol Biol Phys 60:607–612

26. Shirato H, Suzuki K, Sharp GC, et al. (2006) Speed and amplitude of lung tumor motion precisely detected in four-dimensional setup and in real-time tumour-tracking radiotherapy. Int J Radiat Oncol Biol Phys 64:1229–1236

27. Berbeco R, Nishioka S, Shirato H, et al. (2005) Residual motion of lung tumours in gated radiotherapy with external respiratory surrogates. Phys Med Biol 50:3655–3667

28. Sharp GC, Jiang SB, Shimizu S, et al. (2004) Prediction of respiratory tumour motion for real-time image-guided radiotherapy. Phys Med Biol 49:425–440

29. Shirato H, Seppenwoolde Y, et al. (2004) Intrafractional tumor motion: lung and liver. Semin Radiat Oncol 14:10–18

RESEARCH PAPER

Combination tumor immunotherapy with radiotherapy and Th1 cell therapy against murine lung carcinoma

Hiroshi Yokouchi · Kenji Chamoto · Daiko Wakita ·
Koichi Yamazaki · Hiroki Shirato · Tsuguhide Takeshima ·
Hirotoshi Dosaka-Akita · Masaharu Nishimura ·
Zhang Yue · Hidemitsu Kitamura · Takashi Nishimura

Abstract Mice bearing established Lewis lung carcinoma (LLC) expressing model tumor antigen, ovalbumin (OVA) (LLC-OVA) marginally responded to local radiotherapy, but none of the mice was cured. In contrast, treatment of the tumor-bearing mice with intratumoral injection of tumor-specific T helper type 1 (Th1) cells and tumor antigen (OVA) after radiotherapy dramatically prolonged the survival days and induced complete cure of the mice at high frequency (80%). Radiation therapy combined with Th1 cells or OVA alone showed no significant therapeutic activity against LLC-OVA. Such a strong therapeutic activity was not induced by intratumoral injection of Th1 cells plus OVA. Compared with other treatment, radiation therapy combined with Th1 cells and OVA was superior to induce the generation of OVA/H-2^b tetramer$^+$ tumor-specific cytotoxic T lymphocyte (CTL) with a strong cytotoxicity against LLC-OVA in draining lymph node (DLN). Moreover, the combined therapy is demonstrated to inhibit the growth of tumor mass, which grew at contralateral side. These results indicated that radiotherapy combined with Th1 cell/vaccine therapy induced a systemic antitumor immunity. These findings suggested that combination therapy with radiotherapy and Th1 cell/vaccine therapy may become a practical strategy for cancer treatment.

Abbreviations

OVA	Ovalbumin
Th1	T-helper type 1
Ag	Antigen
LLC	Lewis lung carcinoma
CTL	Cytotoxic T lymphocyte
DLN	Draining lymph node
IL	Interleukin
MHC	Major histocompatibility complex
IFN	Interferon
TCR	T cell receptor
MMC	Mitomycin
TIL	Tumor-infiltrating lymphocyte
CT	Computed tomography

Hiroshi Yokouchi and Kenji Chamoto are equally contributed.

H. Yokouchi · K. Chamoto · D. Wakita · H. Kitamura ·
T. Nishimura (✉)
Division of Immunoregulation, Section of Disease Control,
Institute for Genetic Medicine, Hokkaido University, N-15, W-7,
Kita-ku, Sapporo 060-0815, Japan
e-mail: tak24@igm.hokudai.ac.jp

H. Yokouchi · K. Yamazaki · M. Nishimura
First Department of Medicine, Hokkaido University School of
Medicine, Sapporo, Japan

H. Shirato · T. Takeshima
Division of Radiation Oncology, Department of Radiology,
Hokkaido University School of Medicine, Sapporo, Japan

H. Dosaka-Akita
Department of Medical Oncology, Hokkaido University
Graduate School of Medicine, Sapporo, Japan

Z. Yue
Division of ROYCE' Health Bioscience, Section of Disease
Control, Institute for Genetic Medicine, Hokkaido University,
Sapporo, Japan

Introduction

The role of radiotherapy as a treatment of localized cancer is well established. However, it has been demonstrated that

ionizing radiation can render additional negative impact on immune function of cancer hosts. Irradiation directly induces bone marrow suppression, leading to the cytoreduction of the lymphoid system. The elevated levels of tissue-derived TGF-β [1] and IL-10 [2] by irradiation diminish the activity of T-cell immunity specific for tumor antigens [3]. In contrast, irradiation has been also accepted to create an inflammatory setting in vivo via induction of apoptosis and cell surface molecules or upregulation of MHC and costimulatory molecules, thereby modulated the tumor environment for eliciting potent antitumor immunity [4, 5]. Under these circumstances, various investigators have attempted to optimize the use of radiation by combination with immunological properties such as recombinant cytokines [6], cytokine-gene-transduced tumor or virus vaccinations [7, 8], dendritic cells [9, 10], agonistic anti-CD40 monoclonal antibody [11], ex vivo activated cells from draining lymph node (DLN) [12], adoptive transfer of antigen-specific T cells [13, 14] and peritumoral injection of CpG oligodeoxynucleotide [15, 16] in mouse experimental models.

We have previously demonstrated that T-helper type 1 (Th1)-dominant immunity promotes durable cytotoxic T lymphocyte (CTL) responses and exhibits strong protective antitumor immunity in vivo [17–20]. In the series of our experiments, we demonstrated that the mice bearing MHC-class II-negative E.G7 tumor cells treated with systemic Th1 cell therapy combined with intratumoral injection of tumor antigen were completely cured [20]. However, local treatment would be more suitable for clinical purposes because systemic administration of the Th1 cytokine like IL-2 [21], IFN-γ [22] and whole body irradiation have exhibited significant toxicity, though the treatment effect remained unsatisfactory.

Based on these backgrounds, combinatorial treatment with local irradiation and intratumoral injection of antigen-specific Th1 cells was initiated when established tumors became palpable (8–10 mm in diameter). In this paper, we demonstrated that local radiation therapy greatly enhanced the therapeutic efficacy of Th1 cell/vaccine therapy through the generation of tumor-specific CD8$^+$ CTL.

Materials and methods

Mice

Wild-type C57BL/6 mice were obtained from Charles River Japan (Yokohama, Japan). OT-II T cell receptor (TCR)-transgenic mice, expressing a TCR recognizing the dominant I-A^b-restricted OVA epitope ISQAVHAA-HAEINAGR (OVA $_{323-339}$) were kindly provided by F. R. Carbone (University of Melbourne, VIC, Australia).

C57BL/6 mice were all female and used at 5–6 weeks of age. All animal experiments were approved by the committee in our animal institute.

Reagents and monoclonal antibodies

Phycoerythrin (PE) conjugated tetramer of H-2K^b-restricted OVA $_{257-264}$ (SIINFEKL) molecules (OVA-MHC tetramer) was purchased from MBL (Nagoya, Japan). FITC-labeled CD8 mAb were purchased from BD Pharmingen (San Diego, CA). Anti-CD4 mAb-conjugated microbeads for the MACS system were purchased from Miltenyi Biotec (Bergisch Gladbach, Germany). OVA protein was obtained from SIGMA (St. Louis, MO). IL-12 was kindly donated by Dr. Steven H. Herrmann (Wyeth Research Co Ltd, Cambridge, MA). IL-2 was supplied by Ms. Takuko Sawada (Shionogi Pharmaceutical Institute Co Ltd, Osaka, Japan). Anti-IL-4 mAb (11B11) was purchased from American Type Culture Collection (Rockville, MD). Recombinant IFN-γ was purchased from Pepro Tech EC ltd (London, England). OVA $_{323-339}$ peptide was kindly supplied by Dr. H. Tashiro (Fujiya Co Ltd, Hadano, Japan).

Cell culture

Lewis lung carcinoma (LLC) cell line is a mouse lung carcinoma of C57BL/6 origin. The LLC-OVA cell line was derived from LLC by transfection with chicken OVA cDNA. Cells were cultured in Iscove's Modified Dulbecco's Medium (Invitrogen Corp, Carlsbad, CA) supplemented with 10% fetal bovine serum (Invitrogen Corp), L-glutamine, 25 mM N-2-hydroxyethylpiperazine-N'-3-propanesulfonic acid (HEPES) buffer, 0.05 mM 2-mercaptoethanol (2-ME), penicillin and streptomycin. To enhance the expression of MHC class I, LLC cells were treated with 10 ng/ml of IFN-γ for 48 h at 37°C and were washed three times with medium before testing by cytotoxicity assays. T cell lymphoma MBL-2 lymphoma was cultured in RPMI1640 medium (SIGMA) supplemented with 10% fetal bovine serum, 2 mM L-glutamine, 0.05 mM 2-ME, HEPES, penicillin and streptomycin. To prepare OT-II mice derived IFN-γ-producing CD4$^+$ T cells (Th1 cells), CD4$^+$ CD45RB$^+$ naïve T cells were isolated from spleen cells from OT-II mice using FACS Vantage (Becton Dickinson, San Jose, CA) as reported previously [23]. Purified CD4$^+$CD45RB$^+$ cells were stimulated with OVA peptide (5 μg/ml) in the presence of MMC-treated splenocytes from wild-type C57BL/6 mice, anti-IL-4 mAb (50 μg/ml), IL-2 (100 U/ml), IFN-γ (1 ng/ml), and IL-12 (20 U/ml). At 48 h, cells were restimulated with OVA $_{323-339}$ under the same conditions, and used at 9–12 days of culture.

Local irradiation

The mice bearing LLC-OVA were anesthetized, immobilized in a plastic syringe with a hole from which we can pull out the target tumor, and put the mouse under a 8 mm-thick lead shield with a 10 × 10 mm hole. In therapeutic experiments (Figs. 1 and 4), the mouse was locally irradiated with a single dose of 20 Gy (^{60}Co source, Toshiba, Tokyo, Japan, 1 Gy/min) through the hole at Central Institute of Isotope Science, Hokkaido University. In the experiments shown in Figs. 2 and 3, the mouse was locally irradiated with a single dose of 18 Gy (X ray, Toshiba, Tokyo, Japan, 10 Gy/min) through the animal facility of Hokkaido University School of Medicine.

Treatment protocol

Mice were injected intradermally into the right flank at day 0 with 2×10^6 tumor cells per mouse in 150 μl of phosphate-buffered saline (PBS). The mice bearing LLC-OVA were locally irradiated with a single dose of 20 Gy on day 5 when the diameter of inoculated tumor reached around 8–10 mm. Five days after irradiation, the tumor-bearing mice were further treated with intratumoral injection of 2×10^7 OT-II mice-derived Th1 cells with 50 μg OVA antigen in 100 μl of PBS every 2 days for three times. Mice were measured for tumor growth using calipers every other day and tumor volume was calculated by the following formula: tumor volume = 0.4 × length (mm) × [width (mm)]^2 [24]. For contralateral experiments, mice were injected intradermally into both flanks with 2×10^6 LLC-OVA cells each. The right flank of the double tumor-bearing mice were treated with the same therapy as the mice

bearing single tumor, and then tumor volume of both tumors was calculated in the same manner above. Experimental groups consisted of five mice/group.

Tetramer staining

Tumor-infiltrating lymphocytes (TILs) were isolated from tumor tissues using protease (DISPASE, Godoshusei Co Ltd, Tokyo, Japan) followed by Percoll (Amersham Biosciences Corp, Piscataway, NJ) gradient method. We slightly modified the use of OVA-MHC tetramer. Briefly, lymphocytes from lymph nodes and tumor tissues were washed with PBS twice, stained with 2 μl OVA -MHC tetramers per 1×10^6 cells and then incubated at 4°C for 15 min. The cells were again washed with PBS. The cells were stained with FITC-conjugated anti-CD8 mAb at 4°C for 15 min, then subjected to the FACS analysis.

Flow cytometry

Detailed procedures for staining and sorting were described previously [18]. Fluorescence data were collected on a FACSCalibur flow cytometer (Becton Dickinson, San Jose, CA), and analyzed using CellQuest software (BD Biosciences, Mountain View, CA).

Cytotoxicity assay

The cytolytic activity of lymphocytes obtained from DLN was assessed in ^{51}Cr release assays as described previously [18]. Tumor-specific cytotoxicity of the cells was determined using LLC-OVA prepared from established tumors as target cells. LLC-OVA tumor burdens isolated from the
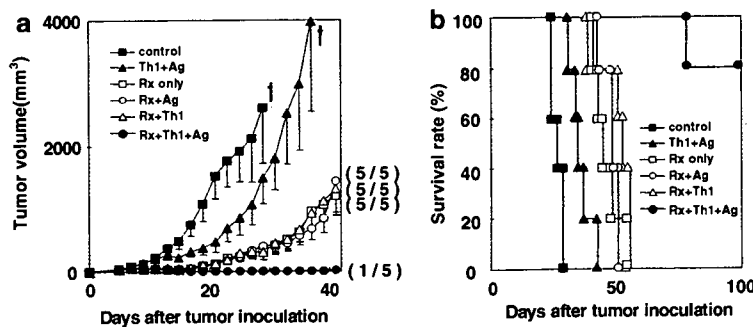

Fig. 1 Local gamma irradiation in combination with intratumoral Th1 cells and antigens eradicate established tumors. LLC-OVA cells (2×10^6) were inoculated intradermally into C57BL/6 mice. When the tumor diameter reached 8–10 mm on day 5, the tumor-bearing mice were treated with various protocols. (a) Tumor-bearing mice were treated with PBS (closed square), or local irradiation (Rx: 20 Gy) only (open square), irradiation with intratumoral injection of OVA protein (Ag: 50 μg) (open circle), irradiation with local administration of Th1 cells (2×10^7) (open triangle), Th1 plus Ag

with (closed circle) or without (closed triangle) irradiation. The antitumor activity induced by the treatment was determined by measuring tumor size in perpendicular diameters. Tumor volume was calculated as described in "Material and methods." The fractional numbers in parenthesis indicate dead mice/total mice within 100 days after tumor inoculation. (b) Survival of mice following various protocols is shown. Similar results were obtained in three separate experiments. Data are presented as the mean ± SE
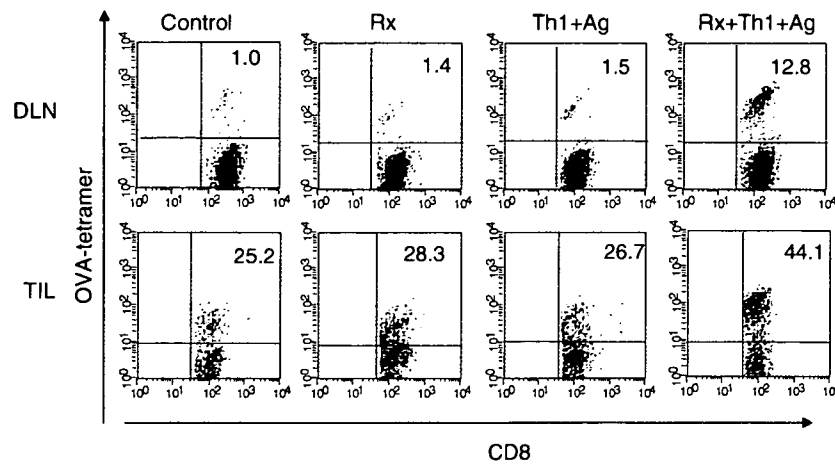
Fig. 2 OVA-MHC tetramer[+] CTLs were efficiently mobilized into both DLNs and tumor tissues from the mice treated with local irradiation and intratumoral administration of Th1 cells plus antigens. LLC-OVA cells (2 × 10^{6}) were inoculated intradermally into C57BL/6 mice and the tumor-bearing mice were treated with various protocols. The tumor was locally irradiated (18 Gy) on day 5, and Th1 cells (2 × 10^{7}) with antigens (50 µg) were administered intratumorally on day 10. DLNs and TILs obtained from the mice treated with indicated therapy on day 18 were labeled with PE-conjugated OVA-MHC tetramer, followed by staining with FITC-conjugated anti-CD8 mAb. About 5,000 CD8^{+} T cells in DLN and 3,000 CD8^{+} T cells in tumor were acquired and analyzed. The numbers indicate the percentage of tetramer-positive cells in the CD8^{+} population. Similar results were obtained in three separate experiments

mice 10 days after inoculation in C57BL/6 mice were minced without using digestive enzymes and incubated on 10 cm plate for 2 h at 37°C, then the supernatant was removed by gently pipetting. Residual adherent cells were harvested by vigorous pipetting and used as targets. As a control, MBL-2 and IFN-γ pre-treated LLC cell lines cultivated in vitro were used. We had already confirmed the expression of MHC-class I on MBL-2 cell lines cultivated in vitro (data not shown). We also had found upregulated expression of MHC-class I molecules on LLC-OVA cells ex vivo, though the expression of in vitro LLC and LLC-OVA cell lines without IFN-γ treatment are extremely weak (data not shown). All cell lines were MHC-class II negative despite of pretreatment with IFN-γ. Pre-labeling of effector cells with OVA-MHC tetramer was used for the purpose of detecting MHC-restricted and antigen-specific cytotoxicities [25]. Briefly, whole DLN cells from the mice treated with combination therapy were labeled with 2 µl OVA-MHC tetramer per 1 × 10^{6} cells and then incubated at 4°C for 15 min. The assay was carried out in triplicate samples at the indicated effector:target ratios (E:T). The percentage of cytotoxicity was calculated as described previously [18].

Results

Local irradiation combined with intratumoral injection of tumor-specific Th1 cells and model tumor antigen induce significant eradication of a well-established LLC-OVA

C57BL/6 mice bearing with lung carcinoma (LLC-OVA) expressing OVA as model tumor antigen were treated with local irradiation (Rx) in combination with intratumoral injection of OVA-specific Th1 cells and OVA model tumor antigens (Ag) (Rx + Th1 + Ag; combination therapy, hereafter). The growth of LLC-OVA was not inhibited by intratumoral injection of Th1 cell therapy alone or antigen alone (data not shown). In three radiotherapy groups (Rx alone, Rx + Ag, Rx + Th1), marginal inhibition of tumor growth was induced. However, none of the mice was cured from tumor. On the other hand, 80% of tumor-bearing mice treated with combination therapy were completely cured from tumor and only one of five mice treated with the combination therapy exhibited the recurrence of tumor growth on day 33 (Fig. 1a). We initially performed the dose searching study of irradiation with fixed dose of Th1 cells and antigen, but none of the treated mice was completely cured from tumor with the irradiation dose under 20 Gy (data not shown). This high dose of local irradiation was well tolerated by virtue of a complete shielding of whole body except for tumor site. In parallel with these results, all the treated mice except for combination therapy died by day 60, while combination therapy induced long-term (day 100) eradication of 80% of the mice (Fig. 1b). These results suggested that combination therapy with irradiation and Th1 cells with antigens induce efficient tumor elimination, leading to long-term survival with acceptable feasibility.
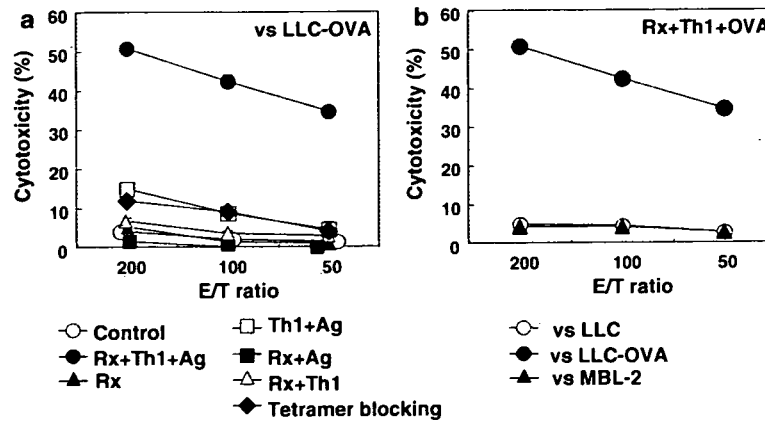
Fig. 3 Tumor-specific CTL activity is augmented by local irradiation in combination with intratumoral Th1 administration and antigens. LLC-OVA cells (2×10^6) were inoculated intradermally into C57BL/6 mice. When the tumor diameter reached 8–10 mm on day 5, the tumor-bearing mice were treated with various protocols. The cells in DLN from the mice treated with various treatments as indicated were harvested on day 18. The harvested cells were used without ex vivo culture in 4 h-^{51}Cr release assay. (a) Cytolytic activities by whole DLN cells from the mice treated with indicated protocols were tested against LLC-OVA. In tetramer blocking assay, whole DLN cells prepared from combination therapy were labeled with OVA—MHC tetramer and the cytotoxic activities were tested against LLC-OVA. (b) CTL activities by whole DLN cells from the mice treated with combination therapy were tested against LLC-OVA (closed circle), LLC (open circle) and MBL-2 (closed triangle). Similar results were obtained in three separate experiments. The bar means ± SE of duplicated samples

Combination tumor immunotherapy with radiotherapy and Th1 cell therapy induces tumor-specific CD8$^+$ T effector cells and systemic antitumor immunity.

The frequency of OVA-MHC tetramer$^+$ CD8$^+$ CTL generation in DLN and tumor tissue of tumor-bearing mice was examined 48 h after second treatment with Rx, Th1 + Ag or Rx + Th1 + Ag. As shown in Fig. 2, both DLN and TIL obtained from mice treated with Rx + Th1 + Ag revealed highest accumulation of tetramer$^+$ CTL compared with other treatment. The frequencies of tetramer$^+$ CD8$^+$ T cells in both draining lymph nodes (DLNs) and tumor tissues obtained from the mice treated with Th1 alone and antigen alone were the same as those from control mice, and the cells from the mice treated with Rx + Ag and Rx + Th1 groups were quite similar to those from Rx alone (data not shown). To investigate whether the lymphocytes in DLN from the mice treated with combination therapy contain cytotoxic effectors, we examined their cytotoxicity against LLC-OVA. As shown in Fig. 3a, whole DLN cells derived from mice treated with the combination therapy exhibited highest cytotoxicity against LLC-OVA compared with those derived from mice treated with none, Rx, Rx + Th1, Rx + Ag or Th1 + Ag. It was also demonstrated that the DLN cells from mice treated with the combination therapy showed tumor-specific cytotoxicity against LLC-OVA but not against LLC, MBL-2 cells (Fig. 3b). Moreover as shown in Fig. 3a, OVA-MHC-tetramer treatment inhibited CD8$^+$ CTL-mediated cytotoxicity against LLC-OVA in the group of combination therapy, which we termed tetramer-blocking assay [25]. These findings demonstrated that the combination

therapy augmented the recruitment of antigen-specific CD8$^+$ T cells, which surely recognized the OVA antigenic peptide bound to MHC Class I (H-2^b), into DLNs and TILs to eradicate tumor tissue in vivo.

Clinical impact of immunotherapy is its possibility of inducing systemic therapeutic effect. To estimate this, we made a double tumor-bearing mouse model. Right flank of the double tumor-bearing mice were treated with the same therapy as the mice bearing single tumor (Fig. 4a), and we examined the growth of contralateral untreated tumor, which was distant from the treated one. Combination therapy significantly suppressed the growth of uninjected tumors. This effect was not found in mice treated with other regimens (Fig. 4b). These results suggest that this combined therapy can establish strong systemic antitumor immunity and it can be applied for the metastatic therapy model.

Discussion

We demonstrated the induction of high complete cure rate of mice bearing mouse lung carcinoma by combined local irradiation and intratumoral administration of antigen-specific Th1 cells with cognate antigen proteins.

Though co-administration of 50 µg OVA antigens was eventually required for the tumor eradication in this treatment, we did not eradicate LLC-OVA cells by using Th1 cells and 200 µg OVA antigens without irradiation (data not shown). These results suggest that irradiation can reduce the requirement of exogenous administration of
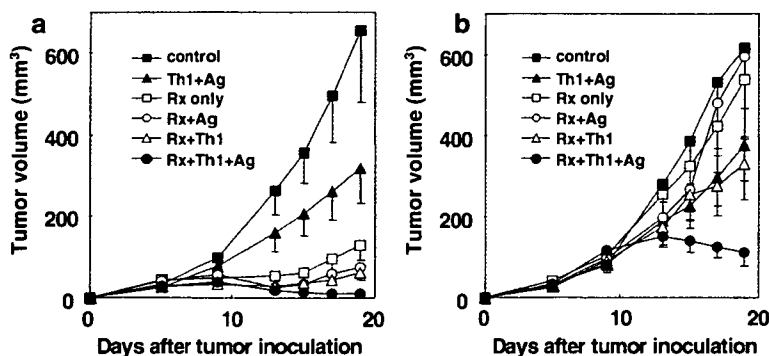
Fig. 4 Local irradiation in combination with Intratumoral administration of Th1 cells and antigens mediates significant regression of contralateral untreated tumors. Mice were injected intradermally with 2×10^6 LLC-OVA cells each in both flanks. On day 5 when the both tumors' diameter reached 8–10 mm, local irradiation only (open square), or irradiation with local administration of antigen (50 µg) (open circle), or irradiation with local administration of Th1 cells

(2×10^7) (open triangle), or Th1 plus OVA antigen with (closed circle) or without (closed triangle) irradiation were treated into established tumors in right flank same as the protocol in Fig. 1. The growth of treated tumor in right flanks and untreated tumor in left flanks were monitored as shown in (a) and (b), respectively. Similar results were obtained in two separate experiments. Data are presented as the mean ± SE

antigens for eliciting antitumor immunity. Recently, a study was reported on the combination of CpG and radiation, showing that CpG was more effective in enhancing the effect of fractionated than single-dose radiation in a mouse model [16]. This efficient protocol seems practical in clinics because the fractionated schedule is commonly used in clinical radiotherapy. Thus, it should be in consideration for the combination of fractionated radiotherapy with Th1 cells in our study. This strategy might enable us to thoroughly reduce exogenous antigens and induce more promising antitumor efficacy.

Recently it has been demonstrated that the frequency of antigen-MHC tetramer is not correlated with the clinical responses [26, 27]. We actually detected tetramer+ CD8+ T cells in DLNs and tumor tissues from the mice of the groups that failed to cure. However, the frequency of tetramer+ CD8+ T cells in DLNs from the mice treated with combination therapy was the highest and significant tumor growth inhibition and high survival rate were observed. Moreover the DLN cells of the mice treated with this therapy killed tumors strongly ex vivo and their cytotoxicity was antigen-specific (Fig. 3). Therefore, this combination therapy enabled us to overcome the tumor defense system with less productivity of immunosupressive regulatory population or with alteration of their tolerized phenotype into activated states. It has been well accepted that generation of antigen-specific Th1 cells is quite difficult and time-consuming. However, we developed an efficient protocol for preparing mouse and human antigen-specific Th1 cells from nonspecifically activated Th1 cells after retroviral transfer of TCR-α and TCR-β genes [28] or lentiviral mediated chimeric immune receptor gene-encoding [29]. We could demonstrate that these antigen-specific artificial Th1 cells expanded in vitro was beneficial for the treatment of cognate tumors in vivo.

We have already established the direct delivery system by which we could mobilize various interventional devises to small peripheral pulmonary lesions of less than 20 mm in diameter using ultrathin bronchoscope under computed tomography (CT) guidance and virtual bronchoscopic navigation [30]. We presume that this method is applicable for the present therapeutic design using intratumoral administration of Th1 cells and/or antigens. Moreover, the radiologists in our university hospital have developed small-volume hypofractionated image-guided radiotherapy without a need for breath control [31]. By this method, the high dose nearly 12 Gy at a time can be applicable for lung cancer patients. They and our colleagues showed its safety and efficiency [32–34]. We showed in this article that the combined therapy led to the induction of systemic antitumor immunity (Fig. 4). Thus we hope the combination therapy could apply to lung metastasis. Although LLC-OVA did not metastasize to other organs, we are now exploring the lung metastatic mice model using other cancers such as B16 melanoma to prove the systemic anti-metastatic efficacy of combined radiotherapy with Th1 cell therapy.

Though further work is required to increase our understanding of the tumor eradication mechanism and to investigate the best protocol design, we hope the results of this experiment will be a rationale study for future clinical trials. Combined radiotherapy with Th1 cell therapy may become a next practical strategy against advanced cancer patients.

References

1. Canney PA, Dean S (1990) Transforming growth factor beta: a promoter of late connective tissue injury following radiotherapy? Br J Radiol 63(752):620–623

2. Broski AP, Halloran PF (1994) Tissue distribution of IL-10 mRNA in normal mice. Evidence that a component of IL-10 expression is T and B cell-independent and increased by irradiation. Transplantation 57(4):582–592

3. Horwitz DA, Zheng SG, Gray JD (2003) The role of the combination of IL-2 and TGF-β or IL-10 in the generation and function of CD4$^+$ CD25$^+$ and CD8$^+$ regulatory T cell subsets. J Leuko Biol 74(4):471–478

4. Friedman EJ (2002) Immune modulation by ionizing radiation and its implications for cancer immunotherapy. Curr Pharm Des 8(19):1765–1780

5. Garnett CT, Palena C, Chakarborty M, Tsang KY, Schlom J, Hodge JW (2004) Sublethal irradiation of human tumor cells modulate phenotype resulting in enhanced killing by cytotoxic T lymphocytes. Cancer Res 64(21):7985–7994

6. Dybal EJ, Haas GP, Maughan RL, Sud S, Pontes JE, Hillman GG (1992) Synergy of radiation therapy and immunotherapy in murine renal cell carcinoma. J Urol 148(4):1331–1337

7. Lumniczky K, Desaknai S, Mangel L, Szonde B, Hamada H, Hidvegi EJ, Safrany G (2002) Local tumor irradiation augments the antitumor effect of cytokine-producing autologous cancer cell vaccines in a murine glioma model. Cancer Gene Ther 9(1):44–52

8. Hillman GG, Slos P, Wang Y, Wright JL, Layer A, De Meyer M, Yudelev M, Che M, Forman JD (2004) Tumor irradiation followed by intratumoral cytokine gene therapy for murine renal adenocarcinoma. Cancer Gene Ther 11(1):61–72

9. Nikitina EY, Gabrilovich DI (2001) Combination of γ-irradiation and dendritic cell administraion induces a potent antitumor response in tumor-bearing mice: approach to treatment of advanced stage cancer. Int J Cancer 94(6):825–833

10. Teitz-Tennenbaum S, Li Q, Rynkiewicz S, Ito F, Davis MA, McGinn CJ, Chang AE (2003) Radiotherapy potentiates the therapeutic efficacy of intratumoral dendritic cell administration. Cancer Res 63(23):8466–8475

11. Honeychurch J, Glennie MJ, Johnson PWM, Illidge TM (2003) Anti-CD40 monoclonal antibody therapy in combination with irradiation results in a CD8 T-cell-dependent immunity to B-cell lymphoma. Blood 102(4):1449–1457

12. Plautz GE, Inoue M, Shu S (1996) Defining the synergistic effects of irradiation and T-cell immunotherapy for murine intracranial tumors. Cell Immunol 171(2):277–284

13. Ganss R, Ryschich E, Klar E, Arnold B, Hammerling GJ (2002) Combination of T-cell therapy and trigger of inflammation induces remodeling of the vasculature and tumor eradication. Cancer Res 62(5):1462–1470

14. Cao ZA, Daniel D, Hanahan D (2002) Sub-lethal radiation enhances anti-tumor immunotherapy in a transgenic mouse model of pancreatic cancer. BMC cancer 2:11

15. Milas L, Mason KA, Ariga H, Hunter N, Neal R, Valdecanas D, Krieg AM, Whisnant JK (2004) CpG oligodeoxynucleotide

16. Mason KA, Ariga H, Neal R, Valdecanas D, Hunter N, Krieg AM, Whisnant JK, Milas L (2005) Targeting toll-like receptor 9 with CpG oligodeoxynucleotides enhances tumor response to fractionated radiotherapy. Clin Cancer Res 11(1):361–369

17. Nishimura T, Iwakabe K, Sekimoto M, Ohmi Y, Yahata T, Nakui M, Sato T, Habu S, Tashiro H, Sato M, Ohta A (1999) Distinct role of antigen-specific T helper type 1 (Th1) and Th2 cells in tumor eradication in vivo. J Exp Med 190(5):617–628

18. Nishimura T, Nakui M, Sato M, Iwakabe K, Kitamura H, Sekimoto M, Ohta A, Koda T, Nishimura S (2000) The critical role of Th1-dominant immunity in tumor immunology. Cancer Chemother Pharmacol 46(Suppl):S52–61

19. Chamoto K, Kosaka A, Tsuji T, Matsuzaki J, Sato T, Takeshima T, Iwakabe K, Togashi Y, Koda T, Nishimura T (2003) Critical role of the Th1/Tc1 circuit for the generation of tumor-specific CTL during tumor eradication in vivo by Th1-cell therapy. Cancer Sci 94(10):924–928

20. Ikeda H, Chamoto K, Tsuji T, Suzuki Y, Wakita D, Takeshima T, Nishimura T (2004) The critical role of type-1 innate and acquired immunity in tumor immunotherapy. Cancer Sci 95(9):697–703

21. Davis ID, Jefford M, Parente P, Cebon J (2003) Rational approaches to human cancer immunotherapy. J Leuko Biol 73(1):3–29

22. Schiller JH, Pugh M, Kirkwood JM, Karp D, Larson M, Borden E (1996) Eastern cooperative group trial of interferon gamma in metastatic melanoma: an innovative study design. Clin Cancer Res 2(1):29–36

23. Ohta A, Sato N, Yahata T, Ohmi Y, Santa K, Sato T, Tashiro H, Habu S, Nishimura T (1997) Manipulation of Th1/Th2 balance in vivo by adoptive transfer of antigen-specific Th1 or Th2 cells. J Immunol Methods 209(1):85–92

24. Ohta S, Tsukamoto H, Watanabe K, Makino K, Kuge S, Hanai N, Habu S, Nishimura T (1995) Tumor-associated glycoantigen, sialyl Lewis (a) as a target for bispecific antibody-directed adoptive tumor immunotherapy. Immunol Lett 44(1):35–40

25. Yokouchi H, Chamoto K, Wakita D, Noguchi D, Yamazaki K, Dosaka-Akita H, Nishimura M, Ikeda H, Nishimura T (2006) Tetramer-blocking assay for defining antigen-specific cytotoxic T lymphocytes using peptide-MHC tetramer. Cancer Sci 97(2):148–154

26. Lee PP, Yee C, Savage PA, Fong L, Brockstedt D, Weber JS, Johnson D, Swetter S, Thompson J, Greenberg PD, Roederer M, Davis MM (1999) Characterization of circulating T cells specific for tumor-associated antigens in melanoma patients. Nature Med 5(6):677–685

27. Lee KH, Wang E, Nielsen MB Wunderlich J, Migneles S, Connors M, Steinberg SM, Rosenberg SA, Marincola FM (1999) Increased vaccine-specific T cell frequency after peptide-based vaccination correlates with increased susceptibility to in vitro stimulation but does not lead to tumor regression. J Immunol 163(11):6292–6300

28. Chamoto K, Tsuji T, Funamoto H, Kosaka A, Matsuzaki J, Sato T, Abe H, Fujio K, Yamamoto K, Kitamura T, Takeshima T, Togashi Y, Nishimura T (2004) Potentiation of tumor eradication by immunotherapy with T-cell receptor gene-transduced T-helper type 1 cells. Cancer Res 64(4):386–390

29. Gyobu H, Tsuji T, Suzuki Y, Ohkuri T, Chamoto K, Kuroki M, Miyoshi H, Kawarada Y, Kato H, Takeshima T, Nishimura T (2004) Generation and targeting of human tumor-specific Tc1 and Th1 cells transduced with a lentivirus containing a chimeric immunoglobulin T-cell receptor. Cancer Res 64(4):1490–1495

30. Shinagawa N, Yamazaki K, Onodera Y, Miyasaka K, Kikuchi E, Dosaka-Akita H, Nishimura M (2004) CT-guided transbronchial

biopsy using an ultrathin bronchoscope with virtual broncho-scopic navigation. Chest 125(3):1138–1143

31. Shirato H, Shimizu S, Shimizu T, Nishioka T, Miyasaka K (1999) Real-time tumour-tracking radiotherapy. Lancet 353(9161): 1331–1332

32. Fukumoto S, Shirato H, Shimizu S, Ogura S, Onimaru R, Ki-tamura K, Yamazaki K, Miyasaka K, Nishimura M, Dosaka-Akita H (2002) Small-volume image-guided radiotherapy using hypofractionated coplanar, and noncoplanar multiple fields for patients with inoperable stage I nonsmall cell lung carcinomas. Cancer 95(7):1546–1553

33. Harada T, Shirato H, Ogura S, Oizumi S, Yamazaki K, Shimizu S, Onimaru R, Miyasaka K, Nishimura M, Dosaka-Akita H (2002) Real-time tumor-tracking radiation therapy for lung car-cinoma by the aid of insertion of a gold marker using bronc-hofiberscopy. Cancer 95(8):1720–1727

34. Onimaru R, Shirato H, Shimizu K, Kitamura K, Xu B, Fukumoto S, Chang TC, Fujita K, Oita M, Miyasaka K, Nishimura M, Dosaka-Akita H (2003) Tolerance of organs at risk in small-volume hypofractionated, image-guided radiotherapy for primary and metastatic lung cancers. Int J Rad Oncol Biol Phys 56(1):126–135

Ischemic complications associated with resection of opercular glioma

TOSHIHIRO KUMABE, M.D.,[1] SHUICHI HIGANO, M.D.,[2] SHOKI TAKAHASHI, M.D.,[2] AND TEIJI TOMINAGA, M.D.[1]

Departments of [1]Neurosurgery and [2]Diagnostic Radiology, Tohoku University Graduate School of Medicine, Sendai, Japan

Object. Opercular glioma inferolateral to the hand/digit sensorimotor area can be resected safely using a neuronavigation system and functional brain mapping techniques. However, the surgery can still sometimes cause postoperative ischemic complications, the character of which remains unclear. The authors of this study investigated the occurrence of infarction associated with resection of opercular glioma and the arterial supply to this region.

Methods. The study involved 11 consecutive patients with gliomas located in the opercular region around the orofacial primary motor and somatosensory cortices but not involving either the hand/digit area or the insula, who had been treated in their department after 1997. Both pre- and postoperative diffusion-weighted magnetic resonance (MR) imaging was performed in the nine consecutive patients after 1998 to detect ischemic complications. All patients underwent open surgery for maximum tumor resection. Postoperative MR imaging identified infarction beneath the resection cavity in all patients. Permanent motor deficits associated with infarction involving the descending motor pathway developed in two patients. Cadaveric angiography showed that the distributing arteries to the corona radiata were the long insular arteries and/or medullary arteries from the opercular and cortical segments of the middle cerebral artery.

Conclusions. Subcortical resection around the upper limiting sulcus of the posterior region of the insula and wide resection in the anteroposterior and cephalocaudal directions of the opercular region were considered to be risk factors of the critical infarction. Surgeons should be aware that resection of opercular glioma can disrupt the blood supply of the corona radiata, and carries the risk of permanent motor deficits.

KEY WORDS • infarction • complication • glioma • descending motor pathway • operculum • diffusion-weighted imaging

P RECISE localization of a glioma in the frontoparietal opercular region inferolateral to the hand/digit sensorimotor area is now possible using various methods including functional brain mapping techniques, neuronavigation systems, intraoperative MR imaging, and photodynamic diagnosis using various photosensitizers. Therefore, gliomas in this location, even in the dominant hemisphere, can be totally resected without causing permanent neurological deficits.[5,9,11,12] During such procedures, surgical techniques for opercular glioma have concentrated on the identification and preservation of the cortical and subcortical functions.[5,11,12] However, little is known about the ischemic complications that can occur after the resection of an opercular glioma.

Diffusion-weighted MR imaging, which reflects the degree of water diffusion in vivo, is an invaluable tool for the diagnosis of acute stroke and other types of brain injury.[14]

Several potential applications of DW MR imaging in patients with gliomas have been recently investigated, mainly for the evaluation of tumor cellularity.[7,8,16,21] Recently, postoperative DW MR imaging has been proposed as a routine study to identify ischemic complications after resection of the glioma.[15] Diffusion-weighted MR imaging detected abnormalities after resection in approximately two thirds of newly diagnosed gliomas. At our institution, postoperative MR imaging including DW imaging has been performed for nearly 10 years as one of the examinations used to determine the postoperative state of patients after tumor removal and has disclosed evidence of postoperative ischemic complications.

In the present study we investigated the postoperative ischemic complications and DW MR imaging findings in 11 patients with pure opercular gliomas surgically treated during the past 9 years. Microangiography studies of cadavers were also analyzed to identify the blood supply for the corona radiata. Finally, referring to the results of the microangiographic analysis, we tried to determine the risk factors for critical infarction at the corona radiata that were likely to result in permanent motor deficits.

TABLE 1

*Summary of characteristics in 11 cases of opercular glioma**

Case No.	Age (yrs), Sex	Diag-nosis	WHO Grade	Tumor Location	Dominant Hemisphere	Presenting Symptoms	Date of Surgery	State of Anesthesia
1	26, M	A	II	rt face motor area	no	lt facial seizure followed by generalized convulsion	1/23/97	awake
2	31, M	AA	III	lt face/tongue motor area	yes	generalized convulsion	9/11/97	awake
3	68, M	AA	III	rt tongue sensori-motor area	no	lt facial seizure	1/27/98	awake
4	3, M	DNET	I	rt face motor area	no	lt facial seizure	12/16/99	general
5	38, M	AA	III	lt face motor area	yes	lt facial seizure	2/28/00	general
6	69, F	GBM	IV	rt face/tongue sen-sorimotor area	no	lt facial seizure followed by lt hemiconvulsion	1/24/02	general
7	49, M	OA	II	rt tongue sensori-motor area	no	incidental	2/5/02	general
8	21, M	A	II	lt tongue sensori-motor area	no	rt facial seizure followed by generalized convulsion	4/11/02	general
9	38, M	AA	III	rt face motor area	no	lt facial seizure	7/22/02	general
10	34, F	O	II	lt face/tongue motor area	yes	rt facial seizure	4/28/03	awake
11	23, M	AA	III	lt face motor area	yes	loss of consciousness	6/9/05	awake

* A = astrocytoma; AA = anaplastic astrocytoma; DCS = direct cortical stimulation; DNET = dysembryoplastic neuroepithelial tumor; KPS = Karnofsky Performance Scale; O = oligodendroglioma; OA = oligoastrocytoma; SCS = subcortical stimulation; US = ultrasonography; WHO = World Health Organization.

Clinical Material and Methods

Patient Population and Tumor Characteristics

This study included 11 consecutive patients, nine males and two females with ages from 3 to 69 years (mean 36.4 ± 19.8 years). Each patient harbored a newly diagnosed glioma located at the opercular region around the orofacial primary motor and somatosensory cortices but not involving either the hand/digit area or the insula and treated in our department after 1997. The tumors included one dysembryoplastic neuroepithelial tumor, two astrocytomas, one oligoastrocytoma, one oligodendroglioma, five anaplastic astrocytomas, and one GBM. Patient characteristics are summarized in Table 1. Informed consent for this study was obtained from all the patients, and institutional review board approval was waived because of the retrospective nature of the study.

Surgical Procedure and Intraoperative Neurophysiological Monitoring

All patients underwent open surgery for maximum tumor resection. Cortical mapping was performed in eight patients, using electric stimuli of 3 to 12 mA to identify the sensorimotor and language cortices, according to a method described previously.[1-4] Five patients were treated while in an awake condition. Primary speech cortex was identified based on speech arrest or hesitation due to stimulation during counting or object naming by the patient. A frameless stereotactic navigation device (ISG Viewing Wand, ISG Technologies; ViewScope, Elekta IGS; or Vector Vision, BrainLAB) was used in all nine cases after 1998; ultrasonography was used in the initial two cases.

Tumor resection was performed using an Ultrasonic Surgical Aspirator (Sonopet, Miwatec Co., Ltd.). All of the opercular arteries were carefully dissected and preserved. If the tumor infiltrated down to the sylvian fissure, thorough dissection of the affected sylvian fissure was initially performed to identify and preserve the insular and opercular segments of the MCAs.

Only the minimum amount of Surgicel (Ethicon, Inc.) was routinely used for hemostasis. Dexamethasone (4 mg) was given every 6 hours with varied tapering schedules, and the administration of anticonvulsants (typically phenytoin and/or zonisamide) and antibiotics was begun or continued in patients during the immediate postoperative period.

Neuroimaging Studies

All patients underwent preoperative, postoperative, and subsequent follow-up MR imaging at our department. Postoperative imaging was performed within 72 hours of surgery. Data from pre- and postoperative DW MR imaging were available for the nine consecutive patients treated after 1998.

For MR imaging, we used a 1.5-tesla system (Signa Horizon LX CV/i, GE Medical Systems) with a conventional quadrature head coil. We obtained T_1-weighted images before and after Gd administration, T_2-weighted images, and DW images during the same imaging session without repositioning the patient's head. Axial DW images were obtained using fat-suppressed spin echo–echo planar imaging (TR 5000 msec, TE 72 msec, number of excitations 2, slice thickness 6 mm, gap 2 mm, matrix 128 × 128, and field of view 23 × 23 cm) with three orthogonal directional motion-probing gradients (b = 1000 seconds/mm²), followed by automatic generation of isotropic DW images. To evaluate the

TABLE 1

(continued)

Stimulation	Navigation System	Extent of Resection	DW Image	Immediate Postop Outcome	Long-Term Deficit	Follow Up (3/26/06)
DCS	US	total	not examined	lt facial palsy	none	no recurrence, KPS 100
DCS	US	total	not examined	rt facial palsy, dysarthria	slight dysarthria	no recurrence, KPS 90
DCS	viewing wand	total	infarction beneath resection cavity	lt hemiparesis	lt fine movement disorder	dead 5/14/99 (dissemination)
none	ViewScope	total	infarction beneath resection cavity	lt hemiparesis	none	no recurrence, KPS 100
DCS & SCS	ViewScope	total	infarction beneath resection cavity	rt facial palsy, dysarthria	slight dysarthria	no recurrence, KPS 90
DCS & SCS	ViewScope	subtotal	infarction beneath resection cavity	lt hemiparesis	lt hemiparesis	dead 4/28/04 (local recurrence & dissemination)
none	ViewScope	total	infarction beneath resection cavity	lt facial palsy	none	no recurrence, KPS 100
none	ViewScope	total	infarction beneath resection cavity	none	none	no recurrence, KPS 100
DCS & SCS	ViewScope	total	infarction beneath resection cavity	none	none	no recurrence, KPS 100
DCS & SCS	ViewScope	subtotal	infarction beneath resection cavity	rt facial palsy, dysarthria	dysarthria	no recurrence, KPS 90
DCS & SCS	Vector Vision	subtotal	infarction beneath resection cavity	rt fine movement disorder, dysarthria	none	no recurrence, KPS 100

spatial relationship between the postoperative ischemic lesion and the pyramidal tract, coronal DW images were also obtained using similar conditions, but the motion-probing gradient was applied in only the anteroposterior direction. The pyramidal tracts, which run in the cephalocaudal direction, were delineated as slightly hyperintense to adjacent brain parenchyma in these coronal images.

The extent of the resection was evaluated according to MR images obtained within 72 hours of surgery. If the tumor had been enhanced on the preoperative MR images, its gross-total resection was defined as no residual enhanced tumor, its subtotal resection as more than 75% removal, and its partial resection as less than 75% removal. If the tumor had not been enhanced on the preoperative MR images, resection was evaluated based on the presence of residual high-intensity lesion on the T_2-weighted MR images.

Postoperative Neurological Outcomes

The postoperative neurological outcome was recorded and confirmed by retrospective review of all hospital records and physician notes. Immediate postoperative neurological function was determined during the first 7 days after surgery, and long-term function was determined between 3 and 6 months after surgery.

Microangiographic Analysis of Vascular Supply to the Corona Radiata

Coronal and axial microangiograms of five cadaveric brains without gross brain pathological features, which were part of a microangiographic study on the distribution of the basal perforating arteries that had been conducted by one of the authors (S.T.) in 1985,[17,18] were reanalyzed to examine

pial cortical arteries in and around the insuloopercular region and to identify the blood supply to the corona radiata.

Results

Extent of Resection

Table 1 outlines the extent of resection in each case, as determined by quantitative volumetric analysis using postoperative MR imaging. Gross-total resection of the lesions was accomplished in eight patients (Cases 1–5 and 7–9). Subtotal resection was achieved in three patients (Cases 6, 10, and 11).

Postoperative MR Imaging and Neurological Outcomes

Postoperative DW MR images showed markedly hyperintense areas representing restricted diffusion in all nine patients treated after 1998. These lesions were all contiguous with the resection cavity. The size of the lesions beneath the resection cavity varied from case to case. All lesions appeared as high-intensity areas on T_2-weighted MR images. Similar high-intensity lesions were also depicted on postoperative T_2-weighted images in the two initial patients without DW imaging data.

Details on postoperative neurological deficits are shown in Table 1. Eight patients, all of whom had undergone relatively small areas of resection mostly located in the face motor area, did not suffer impairment of long-tract function after surgery; three patients (Cases 3, 4, and 6) did have impaired long-tract function immediately after surgery. The lesions with restricted diffusion involved the descending motor pathway in these three patients. Tumor was located in the orofacial sensorimotor area in two of these patients
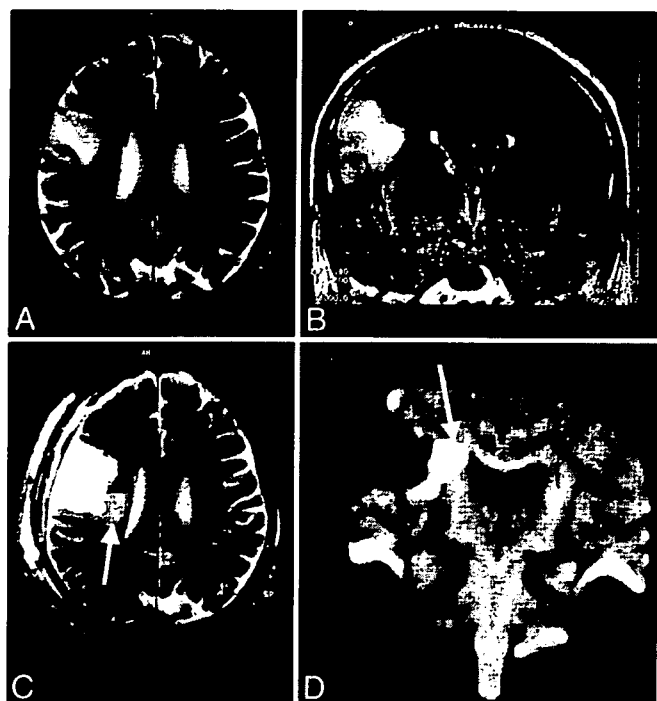
FIG. 1. Case 3. Images obtained in a 68-year-old man with an anaplastic astrocytoma in the right tongue sensorimotor area. Preoperative axial T_2-weighted (A) and coronal fluid-attenuated inversion-recovery (B) MR images revealing a high-intensity mass in the right frontoparietal opercular region. Postoperative axial T_2-weighted (C) and coronal DW (D) MR images showing total removal of the tumor and a new high-intensity lesion (arrows) beneath the resection cavity. The lesion extends to the region of the corona radiata, probably involving the corticospinal tract. This tract appears as a bandlike area of slightly high intensity on the coronal DW image with the motion-probing gradient applied only in the anteroposterior direction.

(Cases 3 and 6). A relatively small resection in these two patients was performed around the white matter above the upper limiting sulcus of the posterior region of the insula, and wide resection was undertaken in the anteroposterior and cephalocaudal directions of the opercular region (Figs. 1–4).

Microangiographic Analysis of Vascular Supply to the Corona Radiata

Coronal microangiography of the cadavers showed that the corona radiata is constantly supplied by the lateral striate arteries, the long insular arteries originating from insular portions of the MCA, and the medullary arteries from the opercular and cortical portions of the MCA (Fig. 5). Surgical removal for opercular glioma, even if not involving the insula, could compromise the latter two fine arteries, resulting in cerebral infarction at the corona radiata.

Illustrative Cases

Case 3

History and Examination. This 68-year-old man presented with an anaplastic astrocytoma manifesting as left facial seizures. Results of T_2-weighted MR imaging demonstrated a hyperintense lesion in the right opercular portions of the inferior frontal, precentral, and postcentral gyri inferolateral to the precentral knob, not involving the insula (Fig. 1A). Administration of a contrast medium caused no enhancement. Neurological and neuropsychological examination revealed no abnormality.

Operation. A right frontoparietotemporal craniotomy was performed with the patient in an awake condition. Direct cortical stimulation identified the face motor area and the primary sensory sites of the tongue and face. The sylvian fissure was thoroughly dissected toward the distal end, and the insular surface was exposed under the operating microscope. The precentral and central arteries were separated from the tumor and preserved. The lesion was totally removed up to the face motor area and toward the deepest portion using the upper limiting sulcus as the anatomical landmark and the ISG Viewing Wand (Fig. 2).

Postoperative Course. Almost complete left hemiparesis was observed postoperatively. Magnetic resonance images showed that the entire lesion had been resected but revealed an ischemic area beneath the resection cavity involving the descending motor pathway (Fig. 1B). As adjuvant therapy, the patient received 72 Gy hyperfractionated radiation to the extended local field. His left hemiparesis resolved except
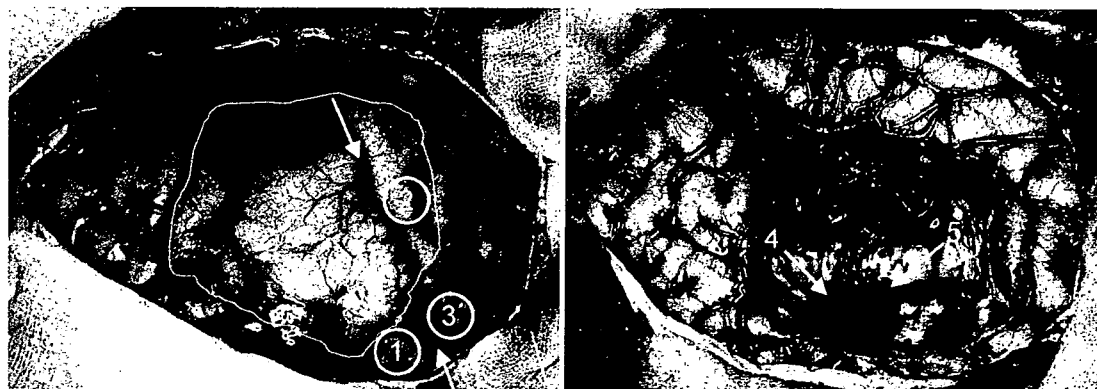

FIG. 2. Case 3. Intraoperative photographs obtained before *(left)* and after *(right)* tumor resection. *Left:* Note the results of functional brain mapping: 1, face motor; 2, tongue sensory; and 3, face sensory. The outline indicates the location of the tumor; the arrows represent the central sulcus. *Right:* Note preservation of the precentral (4) and central (5) arteries.
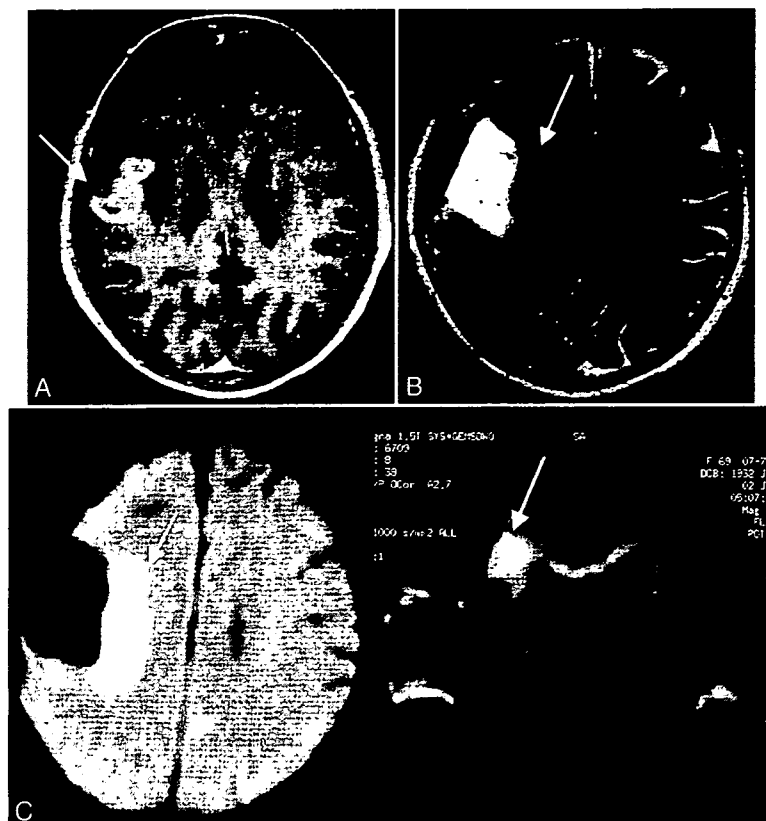
Fig. 3. Case 6. Images obtained in a 69-year-old woman with a right frontoparietal GBM. A: Preoperative axial Gd-enhanced T₁-weighted MR image demonstrating an irregularly enhanced mass lesion in the opercular region around the central sulcus *(arrow).* B: Postoperative axial T₂-weighted MR image depicting total removal of the tumor and a new lesion of high intensity *(arrow)* beneath the resection cavity. C: Postoperative axial *(left)* and coronal *(right)* DW MR images revealing the new lesion *(arrows)* beneath the resection cavity with reduced diffusion probably involving the corticospinal tract.

for impaired fine movement of the left finger. He was discharged home and able to ambulate 2 months postsurgery.

Case 6

History and Examination. This 69-year-old woman presented with a GBM manifesting as left facial seizures followed by left hemiconvulsion. Preoperative T₁-weighted MR images with contrast medium exhibited an enhanced mass in the right opercular portions of the inferior frontal, precentral, and postcentral gyri inferolateral to the precentral knob, not involving the insula (Fig. 3A). Neurological and neuropsychological examination revealed no abnormality.

Operation. A right frontoparietotemporal craniotomy was performed with the patient in a state of general anesthesia. Direct cortical stimulation identified the hand/digit motor area. The sylvian fissure was thoroughly dissected toward the distal end, and the insular surface was exposed under the operating microscope. The precentral, central, and anterior parietal arteries were separated from the tumor and preserved. The lower portion of the lesion was resected toward the deepest portion by using the upper limiting sulcus as the anatomical landmark and the ViewScope. The tumor was removed in a stepwise manner while monitoring the muscle

contraction by direct cortical stimulation to the hand/digit motor area (Fig. 4). The positive cortical response gradually became duller at the end of the surgery.

Postoperative Course. Almost complete left hemiparesis was observed postoperatively. Magnetic resonance images obtained after surgery showed that most of the enhanced lesion had been resected, but an ischemic area was found beneath the resection cavity involving the descending motor pathway (Fig. 3B and C). The patient's left hemiparesis did not resolve.

Discussion

Surgical removal of glioma in the opercular region presents many challenges. In 1991, LeRoux et al.[11] first reported that gliomas involving the nondominant face motor cortex can be safely removed using brain mapping techniques to localize the rolandic cortex and avoid resection of the hand motor cortex and descending subcortical motor pathways. However, resection of the face motor cortex in the dominant hemisphere was not recommended because language localization in the cortical zones is contiguous with this region. In 1995, Ebeling and Kothbauer[5] supposed that radical tumor resection of a purely opercular glioma, not including the insula, in the dominant hemisphere can be

FIG. 4. Case 6. Intraoperative photographs obtained before *(left)* and after *(right)* tumor resection. *Left:* Note the results of functional brain mapping: 1 and 2, hand/digit motor. The *outline* indicates the tumor location; the *arrows* represent the central sulcus. *Right:* Note preservation of the precentral (3), central (4), and anterior parietal (5) arteries.

achieved without significant lasting morbidity. However, only biopsy was recommended for large dominant insular or opercular–insular tumors, because the lenticulostriate arteries hinder total resection and no clear border toward the internal capsule can be found. In 2004, Peraud et al.[12] reported the surgical results of 14 cases of opercular gliomas, stressing the importance of intraoperative neuromonitoring as an aid to surgery in the dominant opercular region. The severity and duration of postoperative deficits was well correlated with the distance from the resection margin to the next positive stimulation point(s), and a distance of more than 5 mm was found to avoid major impairments. Clearly, intraoperative functional brain mapping techniques can help preserve cortical and subcortical functions. However, vascular damage during resection of opercular glioma remains less well understood.

Recently, restricted diffusion abnormalities were found adjacent to the resection cavity on immediately postopera-

tive images in 64% of cases.[15] Both cortical and subcortical lesions with restricted diffusion were observed after surgery. In the present study, postoperative MR images including DW images disclosed infarcted lesions in all patients, and these lesions unexpectedly extended to the descending motor pathway in the corona radiata in three patients, which could have resulted in the impairment of long-tract function. These infarcted lesions were probably caused by disruption of the blood supply during the surgical procedures.

Microangiographic analysis in this study revealed that the corona radiata is supplied by the lateral striate arteries, long insular arteries, and medullary arteries from the opercular and cortical segments of the MCA passing over the frontoparietal operculum. According to the study data collected by Ture et al.,[20] approximately 85 to 90% of insular arteries are short and supply the insular cortex and extreme capsule, 10% are medium length and supply the claustrum and external capsule, and 3 to 5% are long and extend as far

FIG. 5. Coronal *(left)* and axial *(right)* microangiograms of a cadaveric brain slice through the interventricular foramina. Both long insular arteries *(arrows)* arising from the insular portions of the MCA and the medullary arteries *(arrowhead)* from the opercular and cortical portions of the MCA course toward the ventricular wall and supply the region of the corona radiata.